CrossMark

Thickness and Composition Tailoring of K- and Ka-Band Microwave Absorption of $BaCo_xTi_xFe_{(12-2x)}O_{19}$ Ferrites

SUKHLEEN BINDRA NARANG,[1,3] KUNAL PUBBY,[1,4]
and CHARANJEET SINGH[2,5]

1.—Department of Electronics Technology, Guru Nanak Dev University, Amritsar, Punjab, India.
2.—Department of Electronics and Communication Engineering, Rayat and Bahra Institute of
Engineering and Technology, Hoshiarpur, Punjab, India. 3.—e-mail: sukhleen2@yahoo.com.
4.—e-mail: kunalpubby02@gmail.com. 5.—e-mail: charanjeet2003@rediffmail.com

The goal of this research is to investigate the electromagnetic and microwave absorption properties of M-type barium hexaferrites with chemical formula $BaCo_xTi_xFe_{(12-2x)}O_{19}$ (x = 0.0, 0.2, 0.4, 0.6, 0.8, 1.0) in K and Ka band. Characterization techniques such as x-ray diffraction analysis and scanning electron microscopy were applied to confirm ferrite formation. The frequency dependence of the complex permittivity and complex permeability was studied for prepared ferrite samples in the frequency range from 18 GHz to 40 GHz. Factors such as the quarter-wavelength condition, impedance matching, high dielectric–magnetic losses, as well as ferromagnetic resonance were investigated to determine their contribution to the absorption characteristics. It was found that the quarter-wavelength ($\lambda/4$) model could be successfully applied to predict and understand the position as well as number of reflection peaks in the microwave absorption spectrum. The origin of the reflection loss peaks is explained and verified based on calculations of input impedance, loss tangent, and ferromagnetic resonance. Reflection loss analysis revealed that all six compositions exhibited reflection loss peaks (absorption >90%) at their matching thicknesses and frequencies. Therefore, these ferrites are potential candidates for use in electromagnetic shielding applications requiring low reflectivity in K and Ka band.

Key words: Electromagnetic properties, K and Ka band, reflection loss, quarter-wavelength condition, impedance matching, complex thickness

INTRODUCTION

M-type hexaferrites have been widely investigated over the past few decades due to their wide range of technical, industrial, commercial, as well as military applications.[1] Barium hexaferrite ($BaFe_{12}O_{19}$), initially known as ferroxdure, was the first M-type hexaferrite to be characterized, in the early 1950s.[2] Barium hexaferrites (BaM) are ideal magnetic fillers due to their uniaxial magnetocrystalline anisotropy along the c-axis, good chemical stability, low density (5.295 g cm^{-3}),[3] high Curie temperature, high electrical resistivity (10^8 Ω cm),[4] corrosion resistivity, and high magnetic loss. To improve these qualities further, various divalent, trivalent, and tetravalent impurities such as Co–Ti,[5] Co–Ru,[6] Co–Zr,[7] and Al–Cr–Nd[8] have been substituted into their lattice to replace iron. Researchers have also reported successful replacement of barium ions by strontium, lanthanum, or their combination.[9,10] However, the focus of ferrite researchers has mostly been restricted to structural and magnetic characterization. In today's world of technological revolution, the rapid increase in electromagnetic (EM) pollution has motivated analysis of microwave or radar absorbing materials for application in radar stealth technology, ships, tanks, wireless communication, heating

Thickness and Composition Tailoring of K- and Ka-Band Microwave Absorption
of BaCo$_x$Ti$_x$Fe$_{(12-2x)}$O$_{19}$ Ferrites

719

systems, electronic equipment, walls of anechoic chambers, etc. A few researchers have investigated the absorption spectrum of various ferrites in the X band, and a very few in higher bands.[11,12]

The underlying principle used in absorption analysis is the "single-layer metal plate backed absorber model," which makes use of the reflection reduction by impedance matching.[13] Curves of reflection loss (RL) are then simulated for various thicknesses using the following relations for the complex permittivity and permeability:

$$RL(db) = 20 \log \left| \frac{Z_i - Z_o}{Z_i + Z_o} \right| \quad \text{and}$$
$$Z_i = Z_o \sqrt{\frac{\mu_r}{\epsilon_r}} \tanh \left[j \frac{2\pi f d \sqrt{\mu_r \epsilon_r}}{c} \right], \quad (1)$$

where Z_i is the wave input impedance, Z_o is the characteristic impedance (377 Ω), f is the microwave frequency, d is the sample thickness, c is velocity of light in vacuum, ϵ_r is the complex permittivity, and μ_r is the complex permeability. To obtain maximum absorption, two conditions must be satisfied: First, the wave must be incident on the material without front-end reflection, and second, the wave must be attenuated rapidly to a negligible level while propagating inside the material. The first condition ($Z_i = Z_o$) is known as impedance matching and requires equal values of relative permittivity and permeability. However, ferrites have high permittivity and moderate permeability, meaning that exact impedance matching cannot be achieved through dielectric and magnetic resonance alone.[14] In this situation, absorption is achieved by having minimum reflection of EM energy at the material surface, i.e., achieving input impedance as close to the characteristic impedance as possible.[15] Since there is no imaginary part to the characteristic impedance (377 Ω), the input wave must possess impedance with imaginary part close to zero and real part close to 377 Ω. To achieve maximum absorption, the sample thickness is selected according to the quarter-wavelength $\left(\lambda/4 \right)$ model, in which the matching thickness (t_m) depends on the resonance frequency (f_m), complex permeability (μ_r), and complex permittivity (ϵ_r) as follows[16,17]:

$$t_m = \frac{nc}{4 f_m \sqrt{|\epsilon_r \mu_r|}} (n = 1, 3, 5, \ldots), \quad (2)$$

where c is the velocity of light in vacuum. This model has been widely employed to analyze absorption in materials such as Fe$_3$O$_4$ particles,[17] M-type ferrite,[18] W-type ferrite,[19] Z-type ferrite,[20] etc. According to this model, when an electromagnetic wave with a particular frequency impinges on the surface of a metal-plate backed material, the wave is partially reflected from the air–sample interface and partially reflected from the sample–metal interface. For a particular material thickness,

known as the matching thickness (t_m), these reflected waves are 180° out of phase and cancel out, resulting in a reflection dip. Complete characterization of the absorption includes the intensity, location, and bandwidth of this RL dip. The reflection peak must lie in the desired frequency band and also exhibit a large absorption bandwidth.[21] In addition to the thickness, ferromagnetic resonance and electromagnetic losses also affect the peak intensity.

We present herein quantitative characterization of the microwave absorption of BaCo$_x$Ti$_x$Fe$_{(12-2x)}$O$_{19}$ ferrites in the K and Ka band (18 GHz to 40 GHz) along with permittivity and permeability analysis. The obtained results show that these materials are suitable for absorption applications in these frequency bands. The terms "matching frequency" and "matching thickness" used herein refer to the parameters corresponding to the global minimum, although there could also be several local minima.

EXPERIMENTAL PROCEDURES

Barium hexaferrites with structural formula BaCo$_x$Ti$_x$Fe$_{(12-2x)}$O$_{19}$ (x = 0.0, 0.2, 0.4, 0.6, 0.8, 1.0) were prepared by the solid-state reaction route. X-ray diffraction (XRD) analysis was performed on powder samples with the compositions x = 0.4 and x = 0.8 using a Bruker model D8 diffractometer with Cu K$_\alpha$ radiation. The surface morphology of these samples was investigated using a Zeiss Supra 5S scanning electron microscope. Rectangular pellets of these ferrites with thickness of 2 mm were formed from powder after adding polyvinyl alcohol as binder. The complex permittivity (ϵ_r) and complex permeability (μ_r) were characterized by determining the S-parameters using an Agilent N5225A PNA series network analyzer in the K band (18 GHz to 26.5 GHz) and Ka band (26.5 GHz to 40 GHz) at room temperature. Agilent software module 85071 was utilized for determination of electromagnetic parameters.

RESULTS AND DISCUSSION

Crystallographic Characterization

The x-ray diffraction patterns for the powdered samples of BaCo$_{0.4}$Ti$_{0.4}$Fe$_{11.2}$O$_{19}$ and BaCo$_{0.8}$Ti$_{0.8}$Fe$_{10.4}$O$_{19}$ are presented in Fig. 1. Detailed investigation reveals that the diffraction patterns of these samples match well with Joint Committee on Powder Diffraction Standards (JCPDS) standard 430002, revealing formation of a single phase with hexagonal crystal structure. The substitution with Co–Ti resulted in a slight change in peak positions due to variation in lattice parameters. Figure 1 shows a decrease in the intensity of the (0 0 6) reflection peak on increasing x from 0.4 to 0.8, indicating a decrease in the c-axis anisotropy with substitution, while the increase in the intensity of peaks such as (1 1 4) and (2 0 3) indicates
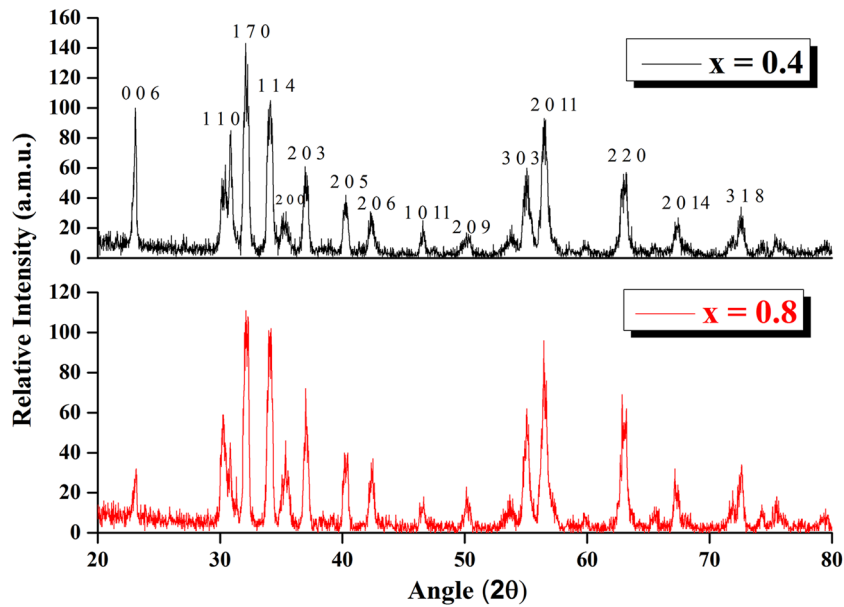
Fig. 1. Typical x-ray patterns for prepared samples with $x = 0.4$ and 0.8 sintered at 1100°C for 6 h.
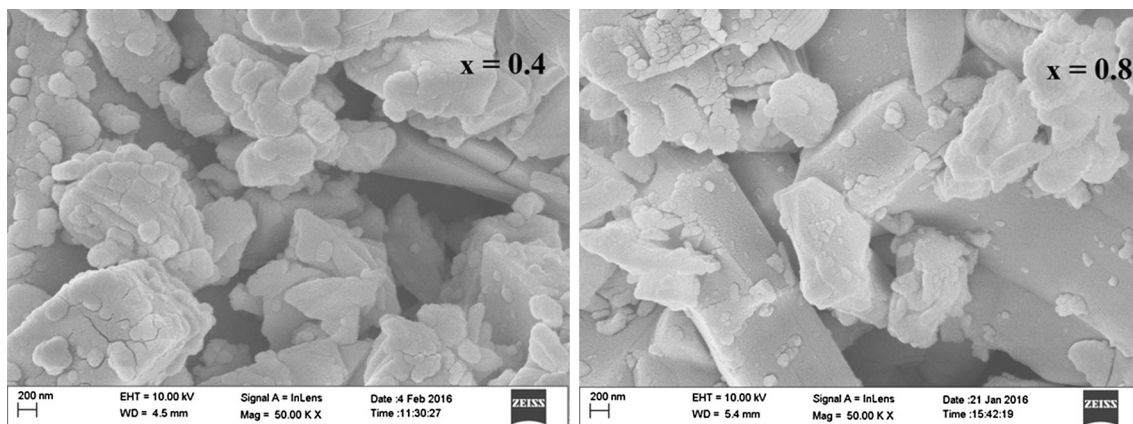

Fig. 2. FE-SEM images of prepared ferrites with $x = 0.4$ and 0.8.

enhancement of the c-plane anisotropy with substitution.[22]

Morphological Evaluation

Figure 2 shows field-emission scanning electron microscopy (FE-SEM) images of Co–Ti-substituted barium hexaferrites. These micrographs show formation and uniform distribution of homogeneous grains. Platelet-shaped grains are formed, being useful for microwave absorption purposes. It is inferred from these images that the mean particle size increased with increasing Co–Ti content, suggesting that the substituted ions acted as grain growth promoters.

Electromagnetic Spectra

The complex permittivity $(\varepsilon_r = \varepsilon' - j\varepsilon'')$ and complex permeability $(\mu_r = \mu' - j\mu'')$ are the two main

factors that together govern the lossy behavior when an electromagnetic wave passes through a ferrite material.[15] The variation of the real part of the permittivity for all the compositions in the series is presented in Fig. 3. In general, the real permittivity spectra show almost constant behavior in the 18 GHz to 26.5 GHz range, and oscillatory behavior in the 26.5 GHz to 40 GHz range. Dong et al.[22] also reported such permittivity behavior in the Ka band. The oscillatory behavior can be justified on the basis that the Ba^{2+} and Fe^{3+} cations, surrounded by O^{2-} ions, contribute to the real and imaginary parts of the permittivity through dipole polarization and dipole relaxation, respectively. The prepared hexaferrites with complex crystalline structure include various cations such as Ba^{2+}, Fe^{2+}, Fe^{3+}, Co^{2+}, and Ti^{4+}, with different coordination numbers. Therefore, dipoles having different relaxation times are formed,[23,24] possibly leading to
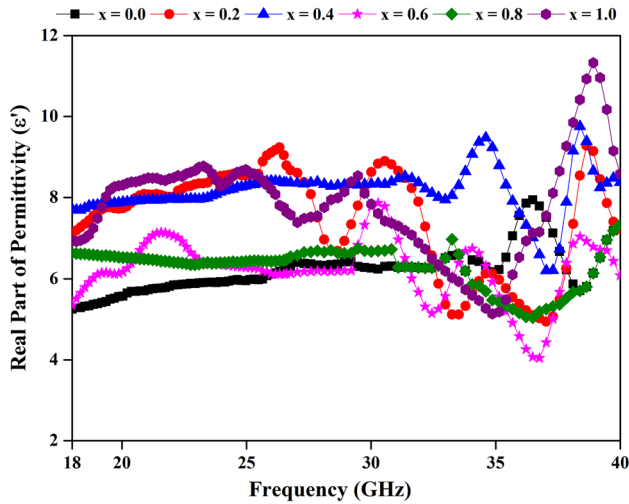
Fig. 3. Frequency and composition dependence of real part of permittivity for different samples in frequency band of 18 GHz to 40 GHz.
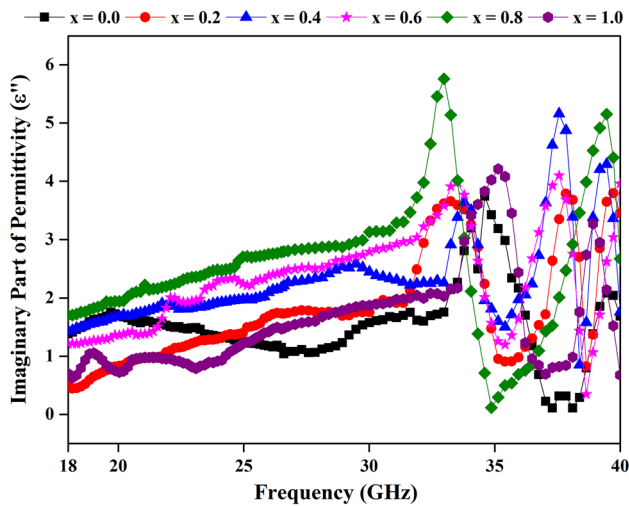

Fig. 5. Real part of the permeability spectra for different ferrite samples in K and Ka band.

Fig. 4. Frequency and composition dependence of imaginary part of permittivity for different samples in frequency band of 18 GHz to 40 GHz.

Fig. 6. Imaginary part of the permeability spectra for different ferrite samples in K and Ka band.

such behavior of the real part of the permittivity in these frequency bands. Similar behavior of ε' was reported earlier in other frequency bands.[23,24] Resonance peaks are observed at the higher side of the Ka band in the ε' spectrum, shifting towards higher frequency (from 36.49 GHz for $x = 0.0$ to 38.38 GHz for $x = 0.4$ and 38.92 GHz for $x = 1.0$) with doping. Also, the resonance peaks in the spectra are observed to widen (increased $\Delta\omega$) with increasing x. As depicted in Fig. 3, the average value of the real permittivity increased with increasing Co–Ti doping, which may be due to the presence of interfacial and dipole polarization due to $Fe^{3+} \leftrightarrow Fe^{2+}$ conversion.[25,26]

Figure 4 shows the variation of the imaginary part of the permittivity (dielectric loss) in the frequency range from 18 GHz to 40 GHz. The
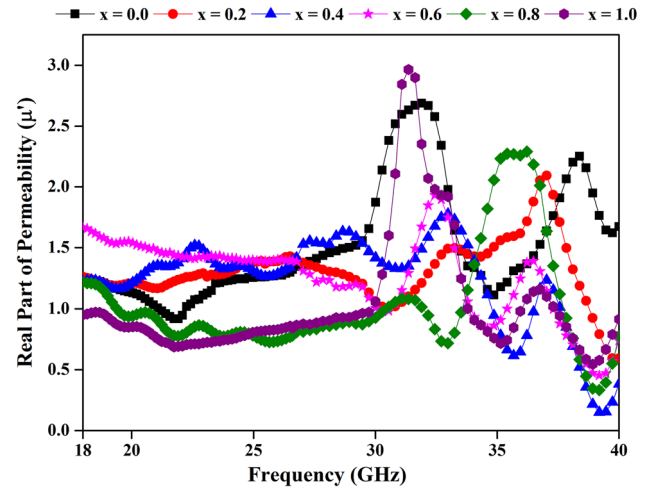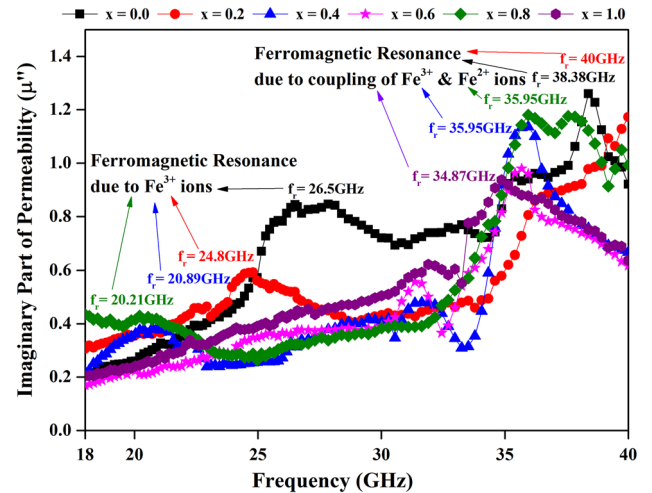
spectrum of the imaginary permittivity also exhibits an oscillatory pattern in the Ka band, while showing a slightly increasing trend in the K band. Similar oscillatory behavior of the loss tangent for M-type hexaferrites in the Ka band has been reported earlier.[22] These losses occur due to damping of vibrations of electrical dipoles, crystal structure, and impurities.[27] These losses are dependent on electron hopping from octahedral to tetrahedral sites and vice versa. The resonance peak is observed at a particular frequency of applied field matching the electron hopping frequency. The resonance peaks observed in the frequency region from 34 GHz to 40 GHz are due to such matching. It was observed that the amplitude of the resonance peaks increased with increasing cobalt–titanium content, which can be attributed to the fact that the imaginary permittivity depends on the number and
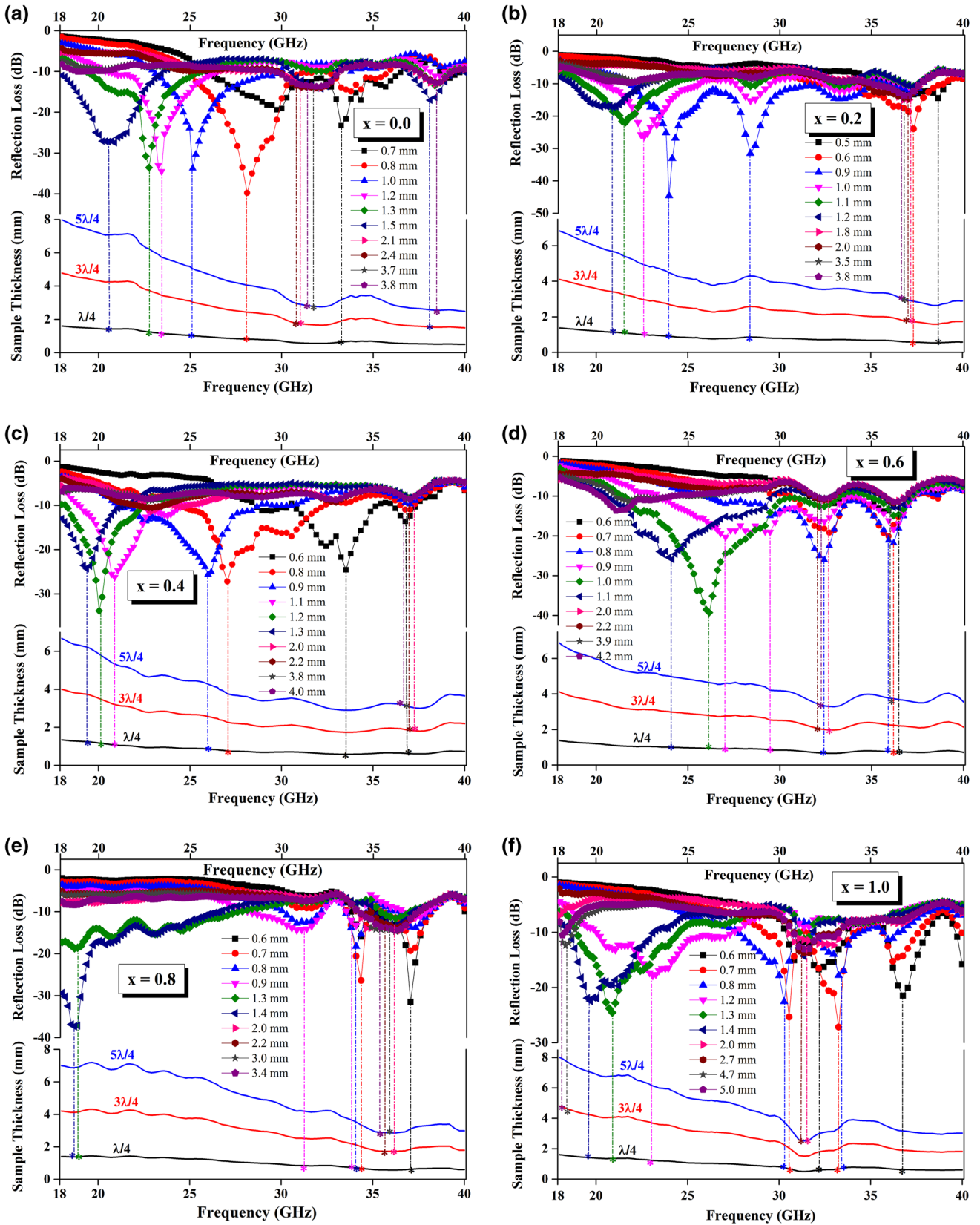
Fig. 7. (a–f) Dependence of reflection loss (db) curves on thickness of ferrite pellets with x = 0.0, 0.2, 0.4, 0.6, 0.8, and 1.0 in K and Ka band (upper part), and satisfaction of quarter-wavelength condition ($t_m = n\lambda/4$ with $n = 1, 3$ and 5) by the thicknesses (lower part). Calculated thicknesses are indicated by star (*) symbols on the $n\lambda/4$ lines.

Table I. Absorption parameters (matching frequency, matching thickness, and reflection loss), ratio of relative permittivity to relative permeability $\left(\left|\varepsilon_r/\mu_r\right|\right)$, normalized input impedance ($|Z_n|$), and real (Z_{Real}) and imaginary (Z_{Imag}) parts of input impedance at the global minimum of reflection loss for the prepared ferrites

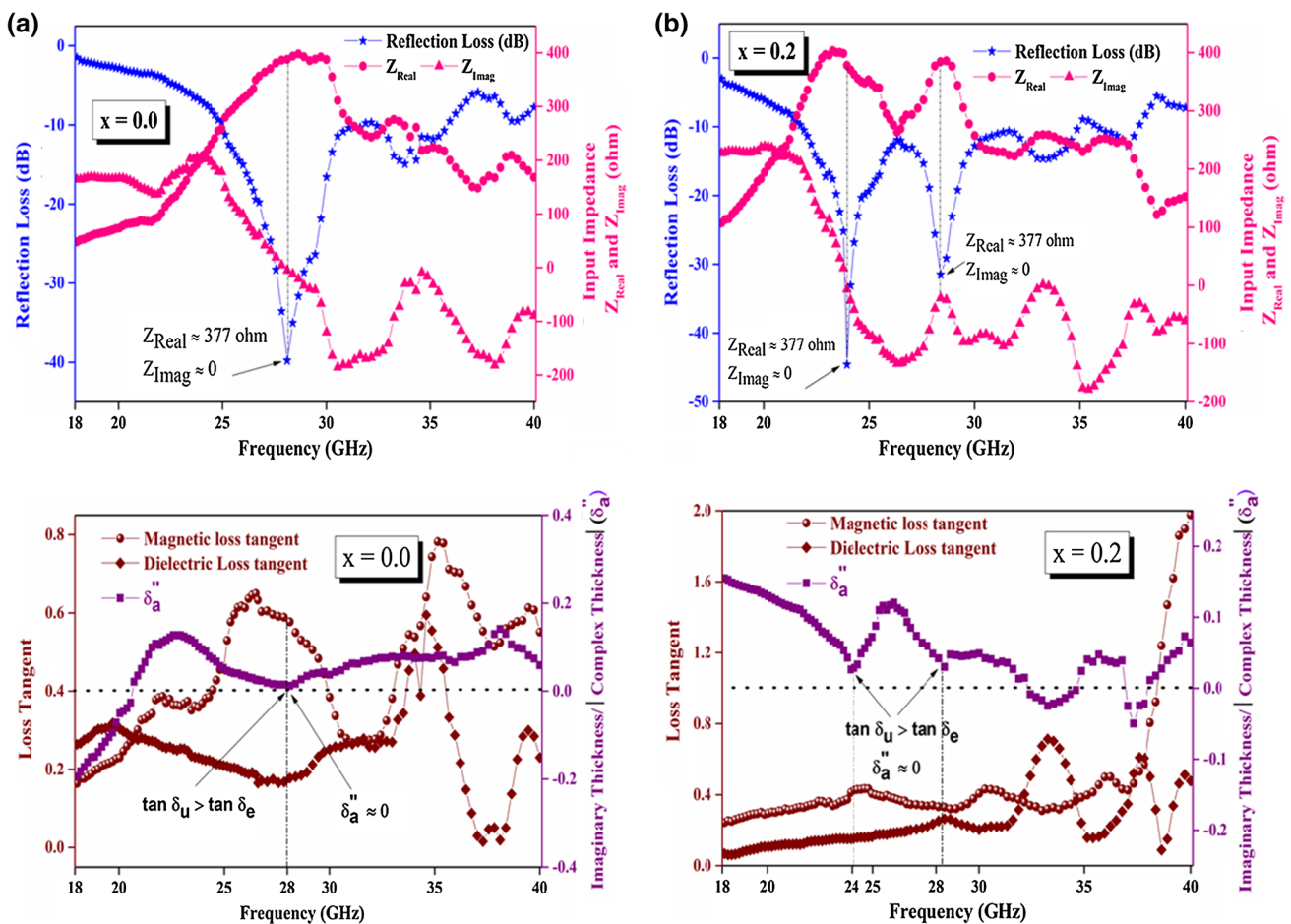| Substitution (x)	Matching frequency (f_m) (GHz)	Matching thickness (t_m) (mm)	Reflection loss at f_m and t_m (dB)	$\left\|\varepsilon_r/\mu_r\right\|$	$\|Z_n\| = \left\|Z_i/Z_o\right\|$	$Z_{Real}(\Omega)$	$Z_{Imag}(\Omega)$
0.0	28.12	0.8	−39.77	3.85	1.027	387.47	0.62
0.2	23.95	0.9	−44.56	6.19	1.003	378.17	−1.53
0.4	20.04	1.2	−33.85	6.45	1.047	394.66	−7.84
0.6	26.16	1.0	−39.29	4.53	0.978	368.63	−0.62
0.8	18.68	1.4	−37.31	5.36	0.982	369.95	14.18
1.0	33.25	0.7	−27.16	3.61	1.080	406.89	15.66

Fig. 8. (a–f) Variation of (top panel) reflection loss, real part of impedance (Z_{Real}) and imaginary part of impedance (Z_{Imag}) and (lower panel) magnetic loss tangent, dielectric loss tangent, and δ_a'' w.r.t. frequency for ferrite pellets with thickness corresponding to minimum reflection loss. This figure indicates that the conditions $Z_{Real} = 377\,\Omega$ and $Z_{Imag} = 0\,\Omega$ and $\tan\delta_u > \tan\delta_e$ correspond to the impedance matching condition ($RL = -\infty$) and result in a global dip in the RL spectra.

nature of the different ions present in the sample.[28] This increase in dielectric loss for the substituted ferrites compared with pure BaM is beneficial for absorption application purposes.

Figure 5 demonstrates the variation of the real part of the permeability with respect to (w.r.t.) frequency for various compositions. The frequency dispersion in the magnetic spectrum is attributed to
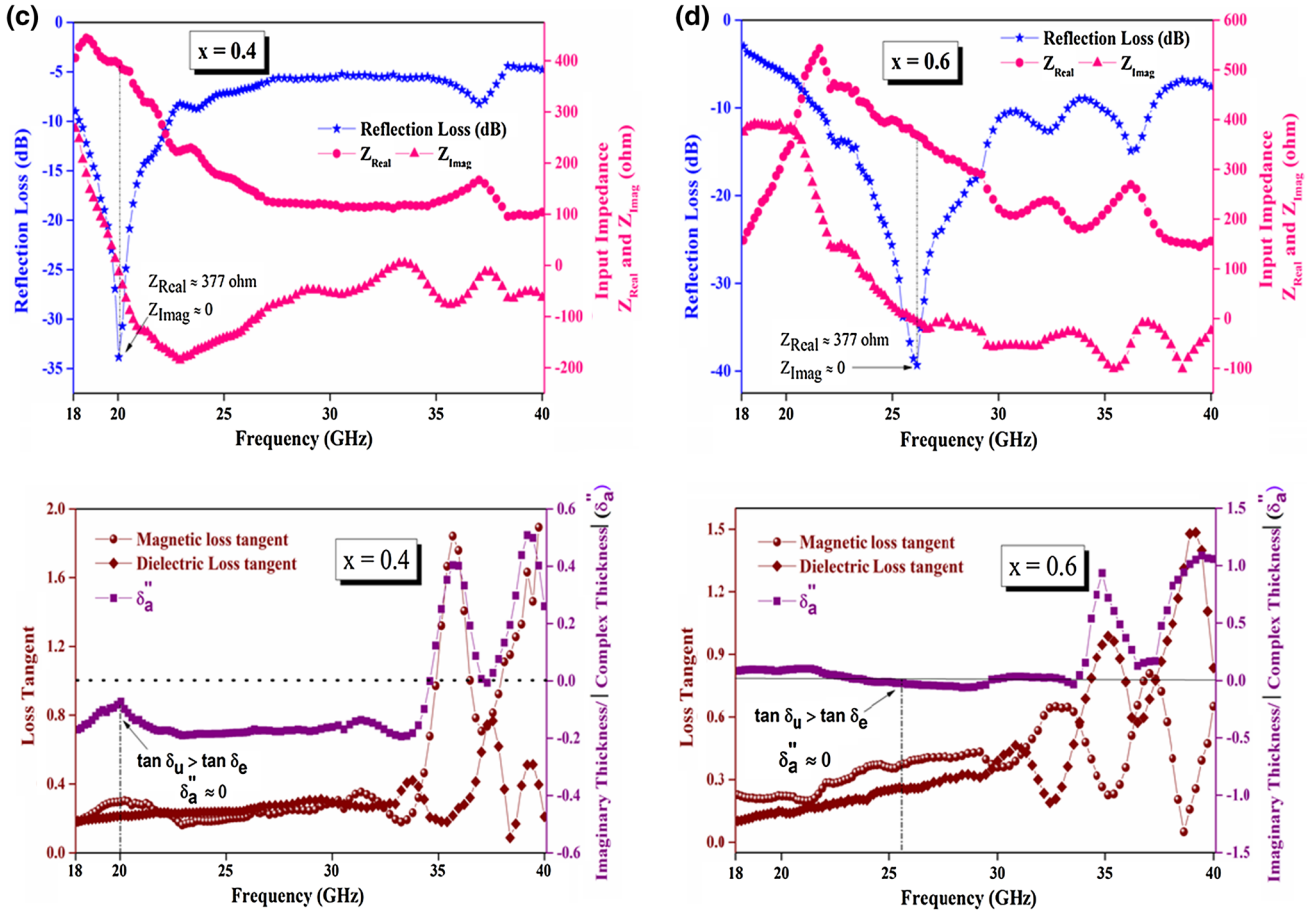
Fig. 8. continued.

two types of magnetizing process: domain-wall turning with relaxation-type dispersion (at the lower side of the frequency band), and natural resonance with resonance-type dispersion (at the higher side of the frequency band).[24] The permeability spectra of the synthesized ferrites contain two resonance peaks in the Ka band, which shift to lower frequency with doping. These resonance peaks can be attributed to the natural resonance mechanism.[29]

The compositional variation of the imaginary part of the permeability (magnetic loss) w.r.t. frequency at room temperature is illustrated in Fig. 6. A slightly increasing trend is observed in the magnetic loss w.r.t. frequency in the K band, while a sharp increase is observed in the Ka band. These spectra show multiple peaks that can be ascribed to the phenomenon of ferromagnetic resonances due to Fe^{3+} ions, Fe^{2+} ions, and their coupling. The ferromagnetic resonance frequency of the ferrites can be calculated from the relation[30]

$$f_r = \frac{\gamma}{2\pi} H_a,$$

where H_a is the anisotropy field and γ is the gyromagnetic ratio ($1.4g$ GHz kOe^{-1}, in which g is the Landé factor, equal to 2 for Fe^{3+} ions, 3.4 for Fe^{2+} ions, and greater than 2 for the coupling). The calculated values of these frequencies are highlighted in Fig. 6, in which the resonance peaks on the lower side correspond to the ferromagnetic resonance due to Fe^{3+} ions and the peaks on the higher side correspond to the resonance due to coupling between Fe^{3+} and Fe^{2+} ions.

Microwave Absorption as Function of Sample Thickness and Substitution

Figure 7a–f (upper part) presents the dependence of the reflection loss (RL) curve on the sample thickness for the compositions with x = 0.0, 0.2, 0.4, 0.6, 0.8, and 1.0. These curves were simulated for the different samples using Eq. 1. It can be inferred that the reflection loss dip shifts to lower frequency as the thickness is increased. This is typical behavior of the RL curve, as observed in other ferrites too.[31] The thickness versus frequency plots (Fig. 7-a–f, lower part) demonstrate the applicability of the quarter-wavelength model ($\lambda/4$ condition) in determining the matching thicknesses of the samples. The lines for $\lambda/4$, $3\lambda/4$, and $5\lambda/4$ are plotted using Eq. 2, while the star (*) points indicate the thicknesses at the particular RL dip calculated using the

Thickness and Composition Tailoring of K- and Ka-Band Microwave Absorption
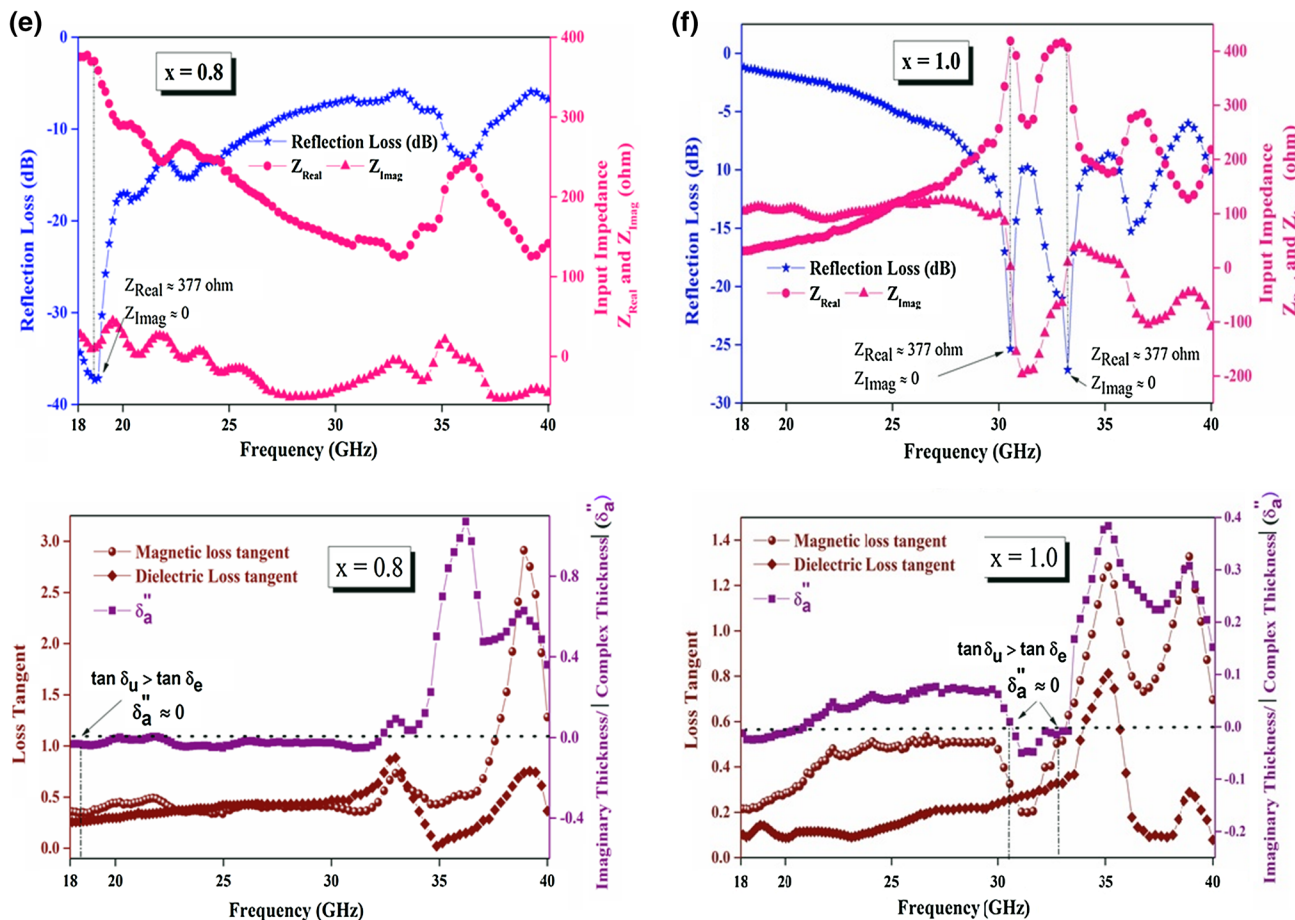of BaCo$_x$Ti$_x$Fe$_{(12-2x)}$O$_{19}$ Ferrites

725

Fig. 8. continued.

quarter-wavelength model. It can be clearly seen that the star points are located reasonably well on these lines, demonstrating that all the absorber thicknesses are in good agreement with the $\lambda/4$ model.[32] However, for a few thicknesses, the RL spectrum exhibits more than one dip, which can be ascribed to matching of impedance at more than one point.[21] The absorption parameters (matching thickness, matching frequency, and reflection loss) corresponding to the global minima in the RL curves are presented in Table I. It can be seen that impedance matching is achieved at situations far from the $|\varepsilon_r/\mu_r| = 1$ condition. This observation differs from earlier reported viewpoints, where "permittivity equal to permeability" is suggested to be a necessary condition for impedance matching. At these frequencies, absorption is achieved by choosing the sample thickness according to the $\lambda/4$ condition.[32]

To explain the origin of the reflection peaks, the variation of the reflection loss for the different samples is plotted at their respective matching thicknesses (indicated in Table I) w.r.t. frequency in Fig. 8a–f. In the lower panel, the magnetic loss tangent and dielectric loss tangent are plotted to reveal their contribution to the electromagnetic

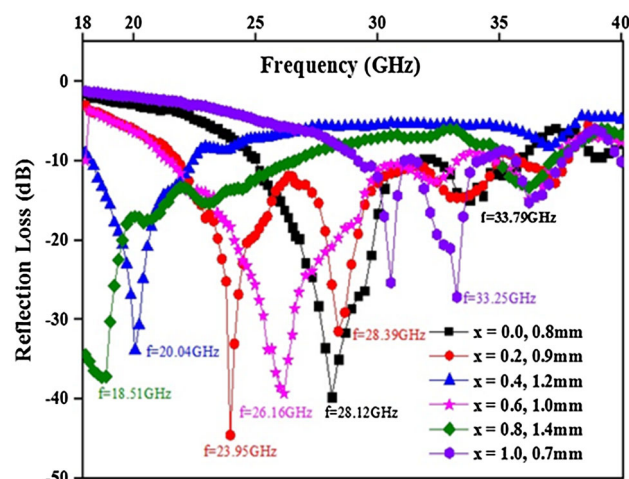Fig. 9. Variation of RL with frequency at thickness corresponding to minimum RL value for each sample.

absorption. Pang et al.[14] reported that δ_a'' can be used to describe the impedance mismatch, being defined as $\delta_a'' = d_a''/|d_a^*|$, where d_a'' is the imaginary thickness and $|d_a^*|$ is the modulus of the complex

Table II. Analysis of factors governing the reflection peaks for $x = 0.2$

Peak frequency (GHz)	Reflection loss (dB) at peak	Quarter-wavelength condition	Impedance matching condition	High dielectric loss	High magnetic loss	Ferromagnetic resonance
23.95	**−44**	Satisfied	Satisfied	No	Yes	Present
28.66	−31	Not satisfied	Satisfied	No	No	Absent
33.25	−13.91	Not satisfied	Satisfied	No	No	Absent
37.3	−12.75	Not satisfied	Not satisfied	Yes	Yes	Absent

The best results of the sample are given in bold.

Table III. Analysis of factors governing the reflection peaks for $x = 0.8$

Peak frequency (GHz)	Reflection loss (dB) at peak	Quarter-wavelength condition	Impedance matching condition	High dielectric loss	High magnetic loss	Ferromagnetic resonance
18.51	**−37.31**	Satisfied	Satisfied	Yes	Yes	Present
36.22	−13.31	Not satisfied	Satisfied	No	No	Absent

The best results of the sample are given in bold.

thickness calculated as $d_a^* = \tanh^{-1}\sqrt{\varepsilon_r/\mu_r}\Big/\big[j2\pi f\sqrt{\mu_r\varepsilon_r}/c\big]$. The smaller the absolute value of δ_a'', the better the impedance matching will be. Along with the loss tangents, δ_a'' is also plotted in the lower panel of Fig. 8a–f. As indicated in the figure, the maximum absorption is observed at the frequency where the magnetic loss tangent is higher than the dielectric loss tangent (i.e., $\tan\delta_u > \tan\delta_e$) and the parameter δ_a'' is close to zero. The points at which the dielectric loss tangent exceeds the magnetic loss tangent have negative δ_a''. The real and imaginary parts of the input impedance are plotted in the top panel of Fig. 8, to explain the impedance matching. The input impedance was calculated at the frequencies corresponding to the RL minima, and it is observed that the real part of the impedance approaches 377 Ω and the imaginary part 0 Ω at those frequencies. This is the requirement to observe RL minima, as stated in the "Introduction." Figure 8a shows that the peak at 28.12 GHz for $x = 0.0$ satisfies all three of these conditions, therefore a global dip is observed at this frequency. Similarly, the other five samples satisfy these conditions at their respective matching frequencies. Local dips are observed in the spectrum at frequencies where any one of these conditions is not satisfied. Due to these local dips, the absorption spectrum of the sample exhibits maxima corresponding to different thicknesses.

To clarify this concept of global and local minima, Fig. 9 shows the variation of the reflection loss for different samples at their respective matching thickness. The sample with $x = 0.2$ exhibits reflection peaks at 23.95 GHz, 28.9 GHz, 34.13 GHz, and 37.3 GHz. The minimum reflection loss of -44 dB is achieved at frequency of 23.95 GHz because the impedance matching and $\tan\delta_u > \tan\delta_e$ conditions are satisfied along with the presence of ferromagnetic resonance. At 28.66 GHz, a reflection peak with comparatively lower magnitude (−31 dB) is observed, because at this position only impedance matching is achieved. Similar reasoning for the other two observed peaks is presented in Table II. The sample with $x = 0.8$ exhibited a RL peak of −37.31 dB at frequency of 18.51 GHz, because all three conditions for high absorption, i.e., impedance matching, high electromagnetic loss, and ferromagnetic resonance, are satisfied at this frequency. The amplitude of the resonance peak at 36.22 GHz is lowered because of the absence of the $\lambda/4$ condition and ferromagnetic resonance (Table III). Similar analysis was also performed for the other samples. Their reflection peaks were also found to originate from one of these phenomena. The position of the primary resonance peak was observed to shift to the lower side of the frequency band with increasing Co–Ti content. Resonance was achieved at 28.12 GHz for $x = 0.0$, while it moved to 23.95 GHz for $x = 0.2$, 20.04 GHz for $x = 0.4$, 26.16 GHz for $x = 0.6$, and 18.68 GHz for $x = 0.8$. This can be attributed to the site occupancy of the impurity ions. When Co–Ti is doped in ferrites, the tetrahedral and trigonal-bipyramidal positions are occupied by Co^{2+} ions while the tetrahedral positions are occupied by Ti^{4+}, strengthening the anisotropy of the crystal face (100).[27] This results in transformation of the anisotropy from axial to planar type, until it becomes in-plane at $x = 1.3$.[33] This non-collinearity causes the variation of the
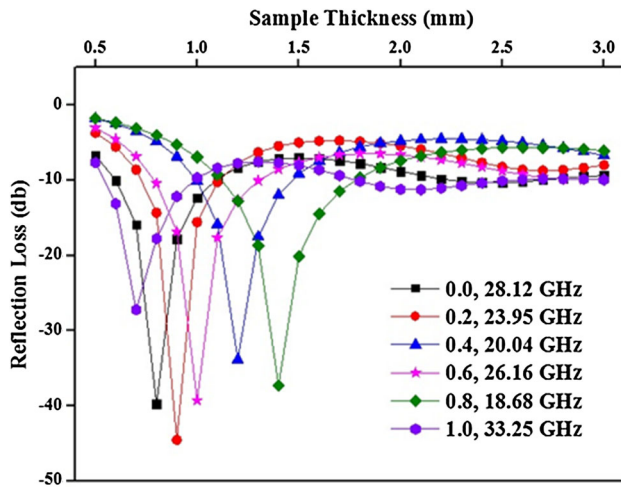
Fig. 10. Variation of RL with pellet thickness at frequencies corresponding to minimum RL values for each sample.

electromagnetic parameters and finally results in the movement of the resonance frequency to lower values.[34] For the sample with $x = 1.0$, the primary resonance frequency might have decreased to the Ku band due to the increased anisotropy field.

Figure 10 shows the variation of RL w.r.t. thickness at the matching frequencies. All the prepared compositions exhibited very high absorption at thicknesses much smaller than the thicknesses reported by Wang et al.[21] and Pang et al.[14] It can be observed that the sample with $x = 0.2$ achieved minimum reflection loss of -44.56 dB at matching frequency of 23.95 GHz and matching thickness of 0.9 mm. Similarly, reflection peaks of -39.77 dB and -39.29 dB were achieved for the samples with $x = 0.0$ and $x = 0.6$ at their matching thicknesses and frequencies. Each composition exhibited its reflection peak at a different thickness as well as different frequency in these frequency bands. This can be attributed to the changes in the anisotropy field as a result of the different amounts of doping.

CONCLUSIONS

The major findings of this investigation are as follows:

1. X-ray diffraction analysis and scanning electron microscopy confirmed synthesis of single-phase ferrites with no significant impurities.
2. Analysis of Co–Ti-substituted barium hexaferrites in the K and Ka band showed that such doping modified the dielectric and magnetic properties of the ferrites.
3. Addition of different amounts of Co–Ti resulted in broadening and amplification of the dielectric and magnetic resonance peaks.

4. Numerical calculations confirmed that the dip in the reflection loss curve was in accordance with the quarter-wavelength model for $n = 1, 3, 5$.
5. A reflection loss peak can be achieved in a desired frequency band by changing the sample thickness, despite the constant permittivity and permeability in a particular frequency band.
6. The quarter-wavelength condition, impedance matching, electromagnetic losses, and ferromagnetic resonance govern the reflection peaks in the absorption spectra of the ferrites.

Thus, the prepared Co–Ti-substituted BaM ferrites are significant for use in practical EM attenuation applications such as EM interference suppression, shielding, EM compatibility testing, and military radars in K and Ka band.

REFERENCES

1. S.B. Narang and I.S. Hudiara, *J. Ceram. Process. Res.* 7, 113 (2006).
2. J.J. Went, G.W. Rathenau, E.W. Gorter, and G.W. Van Oosterhout, *Philos. Technol. Rev.* 13, 194 (1952).
3. International Centre for Diffraction Data, Newton Square, PA, USA PDF No. 84-757.
4. A.E. Van Arkel, E.J.W. Verwey, and M.G. Van Bruggen, *Recl. Trav. Chim.* 55, 331 (1936).
5. S.B. Narang, P. Kaur, S. Bahel, and C. Singh, *J. Magn. Magn. Mater.* 405, 17 (2016).
6. R. Kaur, N. Dhillon, C. Singh, S.B. Narang, and M. Chandra, *Solid State Commun.* 201, 72 (2015).
7. S.B. Narang, S.K. Chawla, R.K. Mudsainiyan, and K. Pubby, *Integr. Ferroelectr.* 167, 98 (2015).
8. M. Jamalian and A. Ghasemi, *J. Supercond. Nov. Magn.* 28, 3293 (2015).
9. C. Singh, S.B. Narang, I.S. Hudiara, K. Sudheendran, and K.C.J. Raju, *J. Magn. Magn. Mater.* 320, 1657 (2008).
10. A. Singh, S.B. Narang, K. Singh, P. Sharma, and O.P. Pandey, *Eur. Phys. J. Appl. Phys.* 33, 189 (2006).
11. E. Kiani, A.S.H. Rozatian, and M.H. Yousefi, *J. Magn. Magn. Mater.* 361, 25 (2014).
12. C. Singh, S.B. Narang, I.S. Hudiara, K. Sudheendran, and K.C.J. Raju, *J. Electroceram.* 27, 120 (2011).
13. J.Y. Shin and J.H. Oh, *IEEE Trans. Magn.* 29, 3437 (1993).
14. H. Pang, M. Fan, and Z. He, *J. Magn. Magn. Mater.* 324, 2492 (2012).
15. A.N. Yusoff, M.H. Abdullah, S.H. Ahmad, S.F. Jusoh, A.A. Mansoor, and S.A.A. Hamid, *J. Appl. Phys.* 92, 876 (2002).
16. T. Inui, K. Konishi, and K. Oda, *IEEE Trans. Magn.* 35, 3148 (1999).
17. I. Kong, S.H. Ahmad, M.H. Abdullah, D. Hui, A.N. Yusoff, and D. Puryanti, *J. Magn. Magn. Mater.* 322, 3401 (2010).
18. S.M. Abbas, R. Chatterjee, A.K. Dixit, A.V.R. Kumar, and T.C. Goel, *J. Appl. Phys.* 101, 074105 (2007).
19. Z.W. Li, G.Q. Lin, Y.P. Wu, and L.B. Kong, *IEEE Trans. Magn.* 45, 670 (2009).
20. Z.W. Li, G.Q. Lin, and L.B. Kong, *IEEE Trans. Magn.* 44, 2255 (2008).
21. B. Wang, J. Wei, Y. Yang, T. Wang, and F. Li, *J. Magn. Magn. Mater.* 323, 1101 (2011).
22. C. Dong, X. Wang, P. Zhou, T. Liu, J. Xie, and L. Deng, *J. Magn. Magn. Mater.* 354, 340 (2014).
23. R.S. Meena, S. Bhattachrya, and R. Chaaterjee, *J. Magn. Magn. Mater.* 322, 2908 (2010).
24. S.M. Abbas, A.K. Dixit, R. Chatterjee, and T.C. Goel, *J. Magn. Magn. Mater.* 309, 20 (2007).

25. J.J. Xu, H.F. Zhou, H.Y. Li, G.H. Li, S.C. Gan, and G.Y. Hong, *J. Alloys Compd.* 490, 552 (2010).
26. F. Guo, G. Ji, J. Xu, H. Zou, S. Gou, and X. Xu, *J. Magn. Magn. Mater.* 324, 1209 (2012).
27. R.C. Pullar, *Prog. Mater. Sci.* 57, 1191 (2012).
28. R.S. Alam, M. Moradi, M. Rostami, H. Nikmanesh, R. Moayedi, and Y. Bai, *J. Magn. Magn. Mater.* 381, 1 (2015).
29. H.J. Zhang, Z.C. Liu, C.I. Ma, X. Yao, and L.X. Zhang, *Mater. Sci. Eng. B Solid B* 96, 289 (2002).
30. S. Ounnunkad, *Solid State Commun.* 138, 472 (2006).
31. D.Y. Kim, Y.C. Chung, T.W. Kang, and H.C. Kim, *IEEE Trans. Magn.* 32, 555 (1996).
32. T. Wang, R. Han, G. Tan, J. Wei, L. Qiao, and F. Li, *J. Appl. Phys.* 112, 104903 (2012).
33. A. Tauber, J.A. Kohn, and R.O. Savage, *J. Appl. Phys.* 14, 1265 (1963).
34. X.F. Yang, Q. Jin, Z.P. Chen, Q.L. Li, and B. Liu, *J. Magn. Magn. Mater.* 367, 64 (2014).